JOURNAL OF COMPUTATIONAL PHYSICS **136,** 337–353 (1997)
ARTICLE NO. CP975739

Numerically Implemented Perturbation Method for the Nonlinear Magnetic Moment of an Anisotropic Superconductor

Igor Žutić and Oriol T. Valls

School of Physics and Astronomy and Minnesota Supercomputer Institute, University of Minnesota, Minneapolis, Minnesota 55455-0149
E-mail: otvalls@maroon.tc.umn.edu, izutic@physics.spa.umn.edu.

Received November 12, 1996

We present a method to compute the magnetic moment of a bulk, finite-size, three-dimensional, anisotropic superconductor. Our numerically implemented perturbative procedure is based on a solution of the nonlinear Maxwell–London electrodynamic equations, where we include the nonlinear relation between current and gauge invariant velocity. The method exploits the small ratio of the finite penetration depths to the sample size. We show how to treat the open boundary conditions over an infinite domain and the continuity requirement at the interface. We demonstrate how our method substantially reduces the computational work required, and discuss its implementation to an oblate spheroid. The numerical solution is obtained from a finite-difference method. We briefly discuss the relevance of this work to similar problems in other fields.

I. INTRODUCTION

A large number of problems in electrodynamics and related areas such as fluid dynamics, involve the solution of partial differential equations for certain fields inside and outside a finite region of a definite geometrical shape. For many common geometries, and when the boundary conditions are simple (e.g., fields or their normal derivatives vanishing at the boundaries) the solution can be found, often with ease, from analytical or simple numerical methods. However, for more complicated situations where one has less trivial boundary conditions, or when the equations are made more complicated by the presence of nonlinearities, analytical methods may be unavailable and numerical techniques encounter serious difficulties.

One of these situations pertains to the electrodynamics of a superconducting sample of finite size. It is well-known that in the limit where the electromagnetic fields do not penetrate the sample the problem can be rather easily solved [1]. However, this is hardly ever the case of interest: the physical information one obtains in experiments comes in fact from the penetration of the fields inside the sample, characterized by penetration depths which, although small, cannot be neglected.

Consider a superconductor that occupies a bounded, macroscopic region $\Omega \subset \mathbf{R}^3$, in the presence of an applied uniform magnetic field, $\mathbf{H}_\mathrm{a}$. For H_a below some critical value, superconductors are in the so called Meissner regime [2], where the magnetic flux is expelled from the bulk of the sample. Their behavior is similar to that of material which is both an ideal conductor and an ideal diamagnet. The applied magnetic field generates a resistance-free current which produces a magnetic field that opposes H_a. As a consequence, everywhere except very close to the interface (within a few penetration depths), the magnetic field vanishes: this is known as the Meissner effect. Except for the most trivial geometries such as infinite slabs or isotropic spheres, the relevant boundary value problem becomes then numerically very awkward: basically one is faced with solving the appropriate electrodynamic equations in the entire space, not just in Ω, while the most important variation of the fields takes place in a very thin boundary layer in Ω.

This question has come recently to the fore in the context of the study of high temperature superconductors (HTSCs). Identifying the symmetry of the paired electrons, the so called pairing state, in these materials, would provide an important clue to the still unknown mechanism responsible for superconductivity in HTSCs. It turns out [3–6] that careful measurements of certain electrodynamic properties in superconductors, can provide fingerprints for the nodal structure of the order (gap) parameter [5] (i.e. the points or lines in the Fermi surface where it vanishes). The unconventional pairing states which are widely believed to exist in HTSCs, produce nonlinearities in the electromagnetic response. As we shall see, the resistance-free current, in addition to the usual terms linear in the superfluid velocity, includes a small contribution for which the current-velocity relation is nonlinear. These nonlinearities then give rise [4, 6], in the Meissner regime, to a magnetic moment which has a small but detectable *transverse* component, $\mathbf{m}_\perp$, perpendicular to the field $\mathbf{H}_\mathrm{a}$ even when this is applied along a direction of symmetry of the sample. This occurs when the applied field lies in the $a-b$ crystallographic plane [7] (the z-axis is taken to be along the c

0021-9991/97 $25.00

crystallographic direction). The angular dependence of the transverse component $m_\perp$, as the crystal is rotated about the z axis, reflects directly the symmetry of the pairing state. It is this quantity that has been experimentally studied [8] for purposes of the identification of the pairing state.

The physics of the situation has been extensively discussed in [6], and we deal here with the mathematical and numerical implications. The computation of the magnetic moment requires the solution of a problem of precisely the kind described in the previous paragraphs. One must solve the appropriate electrodynamics, the Maxwell–London equations described in Section II, for all space, since at infinity the boundary condition requires that $\mathbf{H} \to \mathbf{H}_a$. On Ω these equations contain, as we shall see, important and nontrivial nonlinearities. A solution in the limit of zero penetration of the fields in the sample is possible, but it would be completely inadequate, since it would reflect only the geometry and not the detailed electromagnetic response of the superconductor. On the other hand, the numerical solution for the nonlinear electrodynamics in all space would be computationally demanding.

In this paper we present a discussion of the methods that we have developed to obtain results [6] for the nonlinear magnetic moment, including both the longitudinal and transverse components, in HTSCs. These methods involve the numerical implementation of a perturbation scheme in which the small expansion parameter is the appropriately defined ratio of an effective penetration depth to a characteristic dimension of the superconductor. We will show that this numerical implementation reduces the problem essentially to that of finding the numerical solution in Ω. In the region $\mathbf{R}^3\backslash\Omega$ outside the sample, one turns out to need only a solution for the scalar Laplace equation with trivial Neumann boundary conditions. For a sufficiently symmetric Ω, the form of the solution can be obtained analytically, while for some other cases a numerical solution would suffice.

In Section II we discuss the nonlinear Maxwell–London equations for a superconductor and show how they give rise to the magnetic moment. The geometrical shapes we have considered for Ω (dictated by experimental considerations) are discussed in Section III where we introduce the general solution in $\mathbf{R}^3\backslash\Omega$. In Section IV we discuss the computation of the magnetic moment and present the main result of this paper, the perturbative method and its numerical implementation. Numerical considerations for the equations in Ω are described in the Section V. In Section VI, the equations are solved for the previously discussed geometry, using a modified Gauss–Seidel relaxation, with the nonlinear terms (which are nonanalytic) included through Picard's method. We also illustrate the general ideas of the perturbation method. Finally, in Section VII we give conclusions and guidelines for possible improvements and generalizations. While our discussion is in the context of superconducting electrodynamics, it will not escape the reader's notice that our procedures can be adapted to many other problems in which one is faced with a small "skin depth" or similar parameter involving the penetration of fields or of their derivatives inside a region, and the problem can be more easily solved in the limit where this parameter vanishes.

II. MAXWELL–LONDON ELECTRODYNAMICS

A. *Maxwell–London Equations*

We begin by introducing the steady state Maxwell–London equations [9–11] that provide the framework to compute the field distributions we need in order to evaluate the magnetic moment.

As stated in the Introduction we consider a superconductor in an applied uniform magnetic field $\mathbf{H}_a$ that occupies a bounded simply connected region $\Omega \subset \mathbf{R}^3$ and at its boundary, $\partial\Omega$, is surrounded by vacuum. On $\mathbf{R}^3\backslash\Omega$ the current is $\mathbf{j} = 0$ and therefore in the steady state the local magnetic field $\mathbf{H}$ satisfies the Maxwell equations

$$\nabla \cdot \mathbf{H} = 0 \tag{2.1a}$$

$$\nabla \times \mathbf{H} = 0. \tag{2.1b}$$

The problem reduces to that of finding a magnetic scalar potential Φ that satisfies

$$\mathbf{H} = -\nabla\Phi \tag{2.2a}$$

$$\nabla^2\Phi = 0. \tag{2.2b}$$

On Ω the relevant fields are $\mathbf{H}$, the superconducting current $\mathbf{j}$, and the "superfluid velocity field" $\mathbf{v}_s$ [10] defined as

$$\mathbf{v}_s = \frac{\nabla\chi}{2} + \frac{e}{c}\mathbf{A}, \tag{2.3}$$

where χ is the phase of the superconducting order parameter, $\mathbf{A}$ the vector potential, and e the proton charge, (with $\hbar = k_B = 1$). The field $\mathbf{v}_s$ is conventionally defined as above, and actually has units of momentum. The relation between $\mathbf{v}_s$ and $\mathbf{H}$ is given by the second London equation [10]:

$$\nabla \times \mathbf{v}_s = \frac{e}{c}\mathbf{H}. \tag{2.4}$$

In the steady state the appropriate Maxwell equation is Ampère's law,

$$\nabla \times \mathbf{H} = \frac{4\pi}{c}\mathbf{j}, \tag{2.5}$$

substituting Eq. (2.4) into (2.5) we obtain:

$$\nabla \times \nabla \times \mathbf{v}_s = \frac{4\pi e}{c^2}\mathbf{j}(\mathbf{v}_s) \tag{2.6}$$

which is the general equation that will be investigated in this article. It must be supplemented by a relation, $\mathbf{j}(\mathbf{v}_s)$, which will be discussed in IIC, to be substituted in its right-hand side (RHS). Eq. (2.6) must then be solved together with Eq. (2.2) and the proper boundary conditions.

The required boundary conditions are the following: first at infinity one must have,

$$-\nabla\Phi = \mathbf{H}_a. \tag{2.7}$$

Second, deep inside the sample all fields must vanish. Third, $\mathbf{H}$ must be continuous [9, 11, 12] on the boundary $\partial\Omega$. Finally, the currents are confined to the superconducting material, $\mathbf{j}\cdot\mathbf{n} = \mathbf{0}$ in $\partial\Omega$, $\mathbf{n}$ is the unit normal pointing outwards. The first boundary condition (at an open boundary over an infinite domain) can be satisfied by construction of the solution in $\mathbf{R}^3\backslash\Omega$. The remaining boundary conditions have to be implemented in the numerical algorithm.

Because of these boundary conditions we see that, as emphasized in the Introduction, this problem can indeed be computationally very demanding. It involves solving nonlinear differential equations, in principle in an unbounded region, but with the relevant fields varying very rapidly in a small region inside the material. We will see here and in the next Sections how these difficulties can be overcome, for suitable geometries, by making use of a numerical implementation of a perturbation scheme.

B. *The Magnetic Moment*

Let us at this point introduce some considerations that point to the eventual way out of these numerical difficulties. We recall that the quantity of interest here is the magnetic moment $\mathbf{m}$. From the current distribution $\mathbf{j}$ in Ω, the magnetic moment can be obtained by volume integration [13]

$$\mathbf{m} = \frac{1}{2c}\int_\Omega d\Omega\, \mathbf{r}'' \times \mathbf{j}(\mathbf{r}''), \tag{2.8}$$

where $\mathbf{r}''$ is the position vector for a point in the region Ω.

An important consequence of nonlinear Maxwell–London electrodynamics and unconventional pairing states is that $\mathbf{m}$ need not be aligned with the applied field $\mathbf{H}_a$ even if the latter is applied along a direction of geometrical symmetry, (along a principal axis of the demagnetization tensor [1] of the body). For simplicity, we will restrict ourselves to this case here, although it is straightforward to add the complications arising from a non-diagonal demagnetization tensor.

Let us introduce here, for a typical macroscopic experimental HTSC sample, the ratio between some length d characterizing its size, and the characteristic value of the London penetration depth, which we shall denote by λ. In a macroscopic sample the ratio $\varepsilon = \lambda/d$ is a very small quantity. This small ratio is essentially what will be used in this work to develop a perturbation method to compute the magnetic moment to first order in ε. The starting point of this procedure is the existence of a solution in the limit $\varepsilon \to 0$ (when all the nonlinear effects vanish), which corresponds to imposing trivial Neumann boundary conditions on $\partial\Omega$. For a suitable choice of Ω, such as an ellipsoid, the form of this solution may be found analytically. The perturbation method may also be applied, as we shall see, in certain cases when only a numerical solution in the small ε limit available.

The components of $\mathbf{m}$ parallel and perpendicular to $\mathbf{H}_a$ applied along a direction of symmetry, can generically be written for $\varepsilon \ll 1$ in the form

$$m_\parallel = m_0(1 - \alpha_\parallel\, \varepsilon + O(\varepsilon^2)) \tag{2.9a}$$

$$m_\perp = m_0(\alpha_\perp\, \varepsilon + O(\varepsilon^2)), \tag{2.9b}$$

where m_0 denotes the longitudinal magnetic moment in the limit $\lambda = 0$, (and therefore $\varepsilon = 0$), which is proportional to H_a. It depends only on the geometry of Ω and therefore contains no physical information. For Ω in the shape of an ellipsoid, values are given in [1]. For finite λ there is a reduction, linear in the field to leading order, in the absolute value of $m_\parallel$. This reduction is due to current penetration in the material and it implies a positive constant $\alpha_\parallel$. For a very few simple geometrical shapes and linear, isotropic, Maxwell–London equations, values of $\alpha_\parallel$ are given in textbooks [9, 14]. When nonlinear effects are included, they contribute a correction to $\alpha_\parallel$ linear in the field, but their most conspicuous effect is the appearance, in general, of nonvanishing values of $\alpha_\perp$, also proportional to the field [5, 6]. It is for this reason that the transverse component is the physical quantity of interest.

We next derive an alternative expression for $\mathbf{m}$ that helps to fully exploit the existence of the small parameter ε. Using Eqs. (2.1), (2.5), and formulas for vector calculus [15] one can transform the quantity in the integrand of (2.8):

$$\mathbf{r} \times (\nabla \times \mathbf{H}) = \nabla(\mathbf{r}\cdot\mathbf{H}) - (\mathbf{r}\cdot\nabla)\mathbf{H} - \mathbf{H} \tag{2.10}$$

$$(\mathbf{r}\cdot\nabla)\mathbf{H} = -\nabla \times (\mathbf{r} \times \mathbf{H}) - 2\mathbf{H}. \tag{2.11}$$

After substitution of Eq. (2.11) into Eq. (2.10),

$$\mathbf{r} \times (\nabla \times \mathbf{H}) = \nabla(\mathbf{r}\cdot\mathbf{H}) + \nabla \times (\mathbf{r} \times \mathbf{H}) + \mathbf{H}, \tag{2.12}$$

integration over Ω and use of Gauss' theorem yields

$$\mathbf{m} = \frac{1}{8\pi}\int_{\partial\Omega} dS\,[\mathbf{n}(\mathbf{r}''\cdot\mathbf{H}) + \mathbf{n} \times (\mathbf{r}'' \times \mathbf{H})] + \frac{1}{8\pi}\int_\Omega d\Omega\,\mathbf{H} \equiv \mathbf{m}_1 + \mathbf{m}_2, \tag{2.13}$$

where $\mathbf{r}''$ is the position vector for a point on $\partial\Omega$. The notation $\mathbf{m}_1$, $\mathbf{m}_2$ refers to the two terms in the middle portion of Eq. (2.13). If we recall Eq. (2.4) and use an alternative form of Gauss' theorem we can also rewrite $\mathbf{m}_2$ as a surface integral:

$$\begin{aligned}\mathbf{m}_1 &= \frac{1}{8\pi}\int_{\partial\Omega} dS\,[\mathbf{n}(\mathbf{r}''\cdot\mathbf{H}) + \mathbf{n}\times(\mathbf{r}''\times\mathbf{H})],\\ \mathbf{m}_2 &= \frac{c}{8\pi e}\int_{\partial\Omega} dS\,\mathbf{n}\times\mathbf{v}_s.\end{aligned} \tag{2.14}$$

The terms $\mathbf{m}_1$ and $\mathbf{m}_2$ are of different order in ε and the latter is small, i.e., of $O(\varepsilon m_0)$. This follows from the volume expression for $\mathbf{m}_2$, as seen in Eq. (2.13): since $\mathbf{H}$ is confined to a "skin" layer of thickness λ from the surface, we see at once that $\mathbf{m}_2$ will be of order λ times the applied field, that is, of order εm_0, thus explicitly vanishing in the zero penetration limit. Alternatively, from Eq. (2.4) one sees that $\mathbf{v}_s$ scales as λ and then the same result follows from Eq. (2.14). Specifically if the equations and boundary conditions require the field to decay exponentially far from the surface (up to polynomial corrections), then after decomposing the volume integral into surface and normal components we have

$$\begin{aligned}m_2 &= \frac{1}{8\pi}\int_{S'} dS'\int_0^{w_{\max}} dw\sum_i (H_{\max})_i e^{-(w/\lambda_i)}\\ &\le \frac{3}{8\pi}\mathscr{S}\max(\lambda_i(H_{\max})_i).\end{aligned} \tag{2.15}$$

This expression is not proportional to the volume of Ω, V, as is the case for m_0, but rather to $\lambda\mathscr{S} \sim O(\varepsilon V)$ where $\mathscr{S}$ is the surface area of $\partial\Omega$. As a result m_2 is $O(\varepsilon m_0)$.

C. *The Relation Between* $\mathbf{j}$ *and* $\mathbf{v}_s$

We now return to the pending question of the equation relating the fields $\mathbf{j}$ and $\mathbf{v}_s$ needed to supplement (2.6). This is given by the usual two-fluid phenomenology [5, 6]:

$$\begin{aligned}\mathbf{j}(\mathbf{v}_s) = -eN_f\int_{FS} d^2s\, n(s)\mathbf{v}_f\Big[&(\mathbf{v}_f\cdot\mathbf{v}_s)\\ &+ 2\int_0^\infty d\zeta f(E(\zeta) + \mathbf{v}_f\cdot\mathbf{v}_s)\Big]\end{aligned} \tag{2.16}$$

where N_f is the total density of states at the Fermi level, $n(s)$ is the density of states at point s at the Fermi surface (FS), normalized to unity, $\mathbf{v}_f(s)$ is the s-dependent Fermi velocity, f is the Fermi function, with $E(\zeta) = (\zeta^2 + |\Delta(s)|^2)^{1/2}$, T the absolute temperature and $\Delta(s)$ is the superconducting order (gap) parameter.

In the simplest approximation (which we will call the linear case), one considers only the linear terms in the expression for $\mathbf{j}(\mathbf{v}_s)$, that is, one expands the right side of (2.16) and writes

$$\mathbf{j} = -\frac{c^2}{4\pi e}\tilde{\Lambda}^{-1}\mathbf{v}_s \tag{2.17}$$

where $\tilde{\Lambda}$ is the penetration depth tensor. In the special case of an isotropic superconductor, and *only* in this case, the fields $\mathbf{H}$, $\mathbf{j}$, and $\mathbf{v}_s$ all satisfy the vector Helmholtz equation. But HTSCs are in general highly anisotropic, layered structures with penetration depths much smaller [7] in the layers ($a - b$ planes) than in the direction perpendicular to them (along the c-axis), so that the isotropic limit does not apply. The components of $\tilde{\Lambda}$ in its diagonal representation are the square of the London penetration depths, λ_a, λ_b and λ_c and experimentally $\lambda_c \gg \lambda_a, \lambda_b$. In the numerical examples discussed here we will, for simplicity, neglect the comparatively small in-plane anisotropy and use the notation λ_{ab} for the average of λ_a and λ_b.

In the anisotropic case Eqs. (2.9) are still valid with ε expressed in terms of an effective penetration depth, primarily determined by whichever component λ_i plays the dominant role in the current decay. For example, for the geometry considered in the next Section, the relevant quantity is the penetration depth in the crystallographic $a - b$ plane.

In the problem of interest here one must consider, instead of Eq. (2.17), the nonlinear terms arising from the full relation (Eq. (2.16)) between $\mathbf{j}$, and $\mathbf{v}_s$ and substitute this in the RHS of Eq. (2.6). After suitable assumptions for the FS and other physical quantities are introduced, this can be done by performing the FS integrals numerically, [4] or, in the low temperature limit, analytically [5, 6]. Inclusion of these nonlinear terms is crucial, because, as mentioned, the physically important angular dependence of the transverse magnetic moment arises precisely from these nonlinear effects. The actual expressions for $\mathbf{j}(\mathbf{v}_s)$ used here are taken from [6] and are quoted in Appendix A.

III. ANALYTICAL CONSIDERATIONS: OBLATE SPHEROIDAL GEOMETRY

Experimental samples [16] in which magnetic measurements are performed are in the shape of a flat "disk" with rounded edges, and the axis of revolution along the crystallographic c axis of the crystal. This is well approximated by taking Ω to be a flat ellipsoid of revolution (an oblate spheroid). For an oblate spheroid it is possible to find an analytic expression for the general form of the potential Φ. Therefore, our ideas can be implemented in this geometry in terms of analytic expressions in $\mathbf{R}^3\backslash\Omega$.

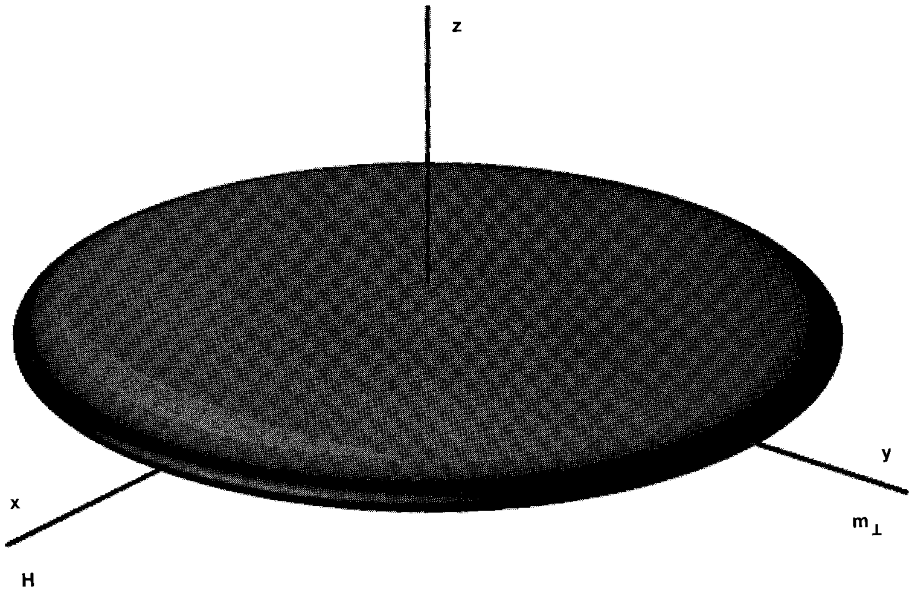

FIG. 1. Geometry considered here. The superconducting region Ω is an oblate ellipsoid of revolution. The x, y, and z directions are fixed in space. The field is applied along the x axis, as indicated, while $\mathbf{m}_\perp$ is along the y axis. The long and short semiaxes values are called A and C in the text, respectively.

The potential Φ, for $\varepsilon = 0$, satisfies trivial Neumann boundary conditions on $\partial\Omega$, and the solution contains a single parameter which is simply related to $m_\parallel$. When the penetration depth is finite, the longitudinal moment does change, but its correct value can in principle be determined from the boundary conditions and the solution inside, either through an iteration process as described in the next Section, or, much more efficiently, through the perturbation method we shall develop.

The fundamental equation (2.6) is not separable in spheroidal coordinates. (Even the vector Helmholtz equation is not.) Still, it is desirable to employ these coordinates as $\partial\Omega$ is then described by a single parameter and this significantly simplifies the process of numerically fulfilling the boundary conditions. The simple implementation and discretization of the boundary conditions on $\partial\Omega$ yields higher accuracy where it is most needed, since boundary grid points lie on the interface.

We denote the major and minor semiaxes of the spheroid by A and C respectively, and we have $A \gg C$ for actual samples. We take (see Fig. 1) a coordinate system fixed to the direction of the magnetic field, with its z-axis parallel to the c crystallographic direction of the superconductor (and parallel to the C semiaxis of an ellipsoid). The field is applied along the x-axis, and we picture the experiment as being performed by rotating the crystal about the z-axis and measuring the angular dependence of $\mathbf{m}_\perp$. As the crystal is rotated the axes $x - y$ remain fixed in space, and should not be confused with the coordinates, affixed to the crystal structure, that we shall also use and denote by x', y'. We call Ψ the angle between axes x and x'.

In the definition we use [17], the oblate spheroidal coordinates ξ, η, φ, are related to Cartesian coordinates by the transformation

$$x = f(1 + \xi^2)^{1/2}(1 - \eta^2)^{1/2} \cos \varphi, \tag{3.1a}$$

$$y = f(1 + \xi^2)^{1/2}(1 - \eta^2)^{1/2} \sin \varphi, \tag{3.1b}$$

$$z = f\xi\eta, \tag{3.1c}$$

where $0 \le \xi < \infty$, $-1 \le \eta \le 1$, $0 \le \varphi \le 2\pi$, and f is a focal length scale factor (the coordinates ξ, η and φ are dimensionless). In Fig. 2 we show this coordinate system at a fixed azimuthal angle $\varphi = 0°$. One can obtain the relation between ξ, η, φ, and Cartesian coordinates fixed to the crystal by replacing φ with $\varphi + \Psi$ in (3.1). For example $x' = f(1 + \xi^2)^{1/2}(1 - \eta^2)^{1/2} \cos(\varphi + \Psi)$. The relation between unit vectors in these and Cartesian coordinates is

$$\hat{\xi} = \frac{1}{(\xi^2 + \eta^2)^{1/2}} (\xi(1 - \eta^2)^{1/2} \cos \varphi\hat{x} + \xi(1 - \eta^2)^{1/2} \sin \varphi\hat{y} + (1 + \xi^2)^{1/2}\eta\hat{z}), \tag{3.2a}$$

$$\hat{\eta} = \frac{-1}{(\xi^2 + \eta^2)^{1/2}} ((1 + \xi^2)^{1/2}\eta \cos \varphi\hat{x} + (1 + \xi^2)^{1/2}\eta \sin \varphi\hat{y} - \xi(1 - \eta^2)^{1/2}\hat{z}), \tag{3.2b}$$

$$\hat{\varphi} = -\sin \varphi\hat{x} + \cos \varphi\hat{y}. \tag{3.2c}$$

We see that $\hat{\xi} = \mathbf{n}$ is the unit normal pointing outwards. In the limit $f \rightarrow 0$, the spheroidal system reduces to the spherical

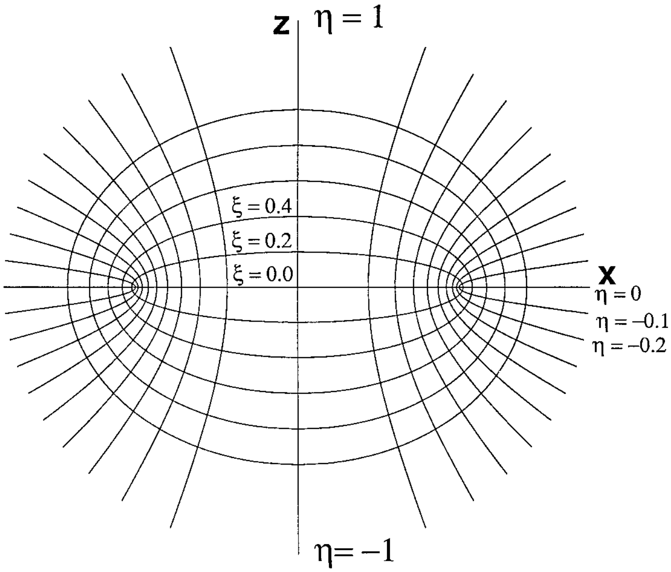

FIG. 2. The relation between oblate spheroidal (ξ, η, φ) and Cartesian coordinates is illustrated at a fixed azimuthal angle $\varphi = 0°$. The surfaces ξ = *constant* and oblate ellipsoids of revolution around the z-axis with semiaxes $A = f(1 + \xi^2)^{1/2}$, $C = f\xi$. The surfaces $|\eta|$ = *constant* are one-sheeted hyperboloids of revolution. The surfaces φ = *constant* are planes through the z-axis making an angle φ with the $x - z$ plane.

coordinate system. For f finite, the surface ξ = const becomes spherical as $\xi \to \infty$:

$$f\xi \to r,\ \eta \to \cos\theta,\ as\ \xi \to \infty. \tag{3.3}$$

In the same limit $\hat{\xi} \to \hat{r}$ and $\hat{\eta} \to -\hat{\theta}$, where r and θ are spherical coordinates. Various quantities in oblate spheroidal coordinates are given in Appendix B.

To construct the general form of the solution for the fields in the region $\mathbf{R}^3\backslash\Omega$ we employ an electrostatic analogy [1]. The current distribution is localized within Ω and the magnetic potential in the exterior region can be written as an expansion in the appropriate set of orthogonal functions which in this case are the spheroidal harmonics [17, 18] (a generalization of spherical harmonics), characterized by angular and azimuthal indices l and m. Thus we write

$$\begin{aligned}\Phi = \Phi_a + \sum_{l=0}^{\infty}\sum_{m=0}^{l} (A_l^m \cos(m\varphi) \\ + A_{l\perp}^m \sin(m\varphi)) f Q_l^m(i\xi)) P_l^m(\eta) \quad \xi \geq \xi_0,\end{aligned} \tag{3.4}$$

where P_l^m and Q_l^m are the associated Legendre functions of the first and second kind respectively, and Φ_a is the potential due to the applied field. The condition that $-\nabla\Phi \to H_a\hat{x}$ when $\xi \to \infty$ yields

$$\Phi_a = -H_a f P_1^1(i\xi) P_1^1(\eta) \cos\varphi. \tag{3.5}$$

Since for $\xi \to \infty$ $Q_l^m(i\xi) \to 0\ \forall m, l$ this fulfills the boundary condition at infinity. The remaining terms in Eq. (3.4) are due to the presence of the superconductor. The coefficients $A_{1\|}^1$ and $A_{1\perp}^1$, for example, multiply terms that give rise to magnetic fields associated with dipole moments along $\mathbf{H}_a$ and perpendicular to it, respectively. In the limit $\varepsilon = 0$ Eq. (3.4) simplifies [1] and the exact solution for Φ is

$$\Phi = \Phi_a + A_{1\|} f Q_1^1(i\xi) P_1^1(\eta) \cos\varphi. \tag{3.6}$$

The parameter $A_{1\|} \equiv A_{1\|}^1$ (for brevity we omit the upper index $m = 1$) is determined from the boundary condition $\partial_\xi\Phi = 0$ at $\xi = \xi_0$, the surface of the spheroid:

$$A_{1\|}(\varepsilon = 0) = \frac{-H_a\xi_0}{1 + 1/(1 + \xi_0) - \xi_0 \arctan(1/\xi_0)}. \tag{3.7}$$

$A_{1\|}$ is always proportional to $m_\|$, the longitudinal magnetic moment. For an ellipsoid, we show in Appendix A that

$$m_\| = \tfrac{2}{3} f^3 A_{1\|}. \tag{3.8}$$

It is instructive to verify that in the linear case the solution on Ω leads to vanishing $m_\perp$. From the linear relation between $\mathbf{j}$ and $\mathbf{v}_s$ in Eq. (2.17) and the anisotropy in $\tilde{\Lambda}$ as discussed in IIC, the azimuthal dependence of $\mathbf{v}_s$ and $\mathbf{j}$ is identical. We can find the φ-dependence of the magnetic moment from Eq. (2.8) and the appropriate element of integration given by Eq. (B6). The φ variable is separable. Consequently, the $\int_0^{2\pi} d\varphi$ integration can be performed analytically and yields $m_\perp = 0$. Thus, any transverse component arises from the nonlinear terms. Their origin can be seen as follows: the superfluid velocity field has, in the presence of nonlinearities, an azimuthal dependence different from that in the linear case. This implies that the φ variable is no longer separable. The nonlinear terms in (A2) lead to higher harmonics for the φ dependence of $\mathbf{v}_s$ on Ω. Then, it follows from Eq. (2.4) that there is a small, but nonvanishing transverse field, $H_\perp$, with a different azimuthal dependence from that in the linear case, which can contribute to $m_\perp$. Therefore the nonlinear response of a superconductor is responsible for $H_\perp$ and, a a result, for $m_\perp$. In $\mathbf{R}^3\backslash\Omega$, the part of $H_\perp$ from which $m_\perp$ arises can be described by a transverse dipole, i.e. a potential of the form of the last term in Eq. (3.6), rotated by 90°

$$\Phi_\perp = A_{1\perp} f Q_1^1(i\xi) P_1^1(\eta) \sin\varphi \tag{3.9}$$

where in full analogy to the longitudinal case in Eq. (3.8)

$$m_\perp = \tfrac{2}{3} f^3 A_{1\perp}. \tag{3.10}$$

The potential $\Phi_\perp$ is the only contribution to $m_\perp$ from the general expression given by Eq. (3.4). This term is small, $A_{1\perp} \ll A_{1\parallel}$ (recall the discussion about $m_\perp/m_\parallel$ from subsection IIB) and does not exist when the penetration depths vanish, since the nonlinear effects are absent unless the field can penetrate the sample. Higher order multipole terms ($l > 1$), as in (3.4) do not contribute to the magnetic moment as can be seen from symmetry considerations or by explicit calculation using the orthogonality of $P_l^m(\eta)$.

It is useful to recall explicitly the connection of the A_l^m with the coefficients in a standard multipole expansion. In the spherical limit given by Eq. (3.3) these coefficients represent ordinary spherical multipoles. For large enough distances from Ω the asymptotic form of the $l = 1$ term is always a pure dipole. The spherical limit of Eq. (3.6) is

$$\Phi = -H_a r \sin\theta\cos\varphi + \frac{m_0}{r^2}\sin\theta\cos\varphi = -H_a x + \frac{m_0 x}{r^3}, \tag{3.11}$$

with

$$m_0 = -\tfrac{1}{2}H_a a^3 \tag{3.12}$$

where a is the sphere radius and we see once more that $A_{1\parallel}(\varepsilon = 0)$ is proportional to m_0.

For finite ξ (not necessarily in the spherical limit), the magnetic moment of a spheroid is again obtained only from terms with $l = 1$ in the Eq. (3.4). The $l = 1$ terms, however, have spheroidal symmetry and their radial and angular dependence is not identical to $1/r^2 \sin\theta$ as for a pure dipole in Eq. (3.11), they have an admixture of higher spherical multipoles.

At finite $\tilde{\Lambda}$ the value for $A_{1\parallel}$ (proportional to $m_\parallel$ from (3.8)) will be slightly different from $A_{1\parallel}(\varepsilon = 0)$, reflecting the difference between $m_\parallel$ and m_0 given by Eq. (2.9a). The potential will also acquire additional terms as seen in Eq. (3.4). The longitudinal terms with $l \geq 2$ and all of the transverse terms vanish at $\tilde{\Lambda} = 0$, that is, they are of higher order in ε. They also vanish in the spherical case but only if $\tilde{\Lambda}$ is isotropic and the relation $\mathbf{j}(\mathbf{v}_s)$ is purely linear. If, in addition, one includes the nonlinear terms in $\mathbf{j}(\mathbf{v}_s)$, so that the full relation (3.4) applies, then the transverse dipole term appears even in a spherical geometry.

IV. COMPUTATION OF THE MAGNETIC MOMENT

A. *General Considerations on Iteration Procedure*

The considerations from the previous section point to a method for obtaining a complete solution for $\mathbf{m}$. This method, although it should work in principle, would naively lead to the need for an iteration which is in practice too cumbersome, and which we discuss here as motivation for introducing the perturbation method obviating the need for it. The important question here is that of calculating the magnetic dipole moment. In other boundary value problems to which our method can be extended, one must similarly determine the lowest nonvanishing multipole moments.

To obtain a solution to Eq. (2.6) in the general case when the relation between $\mathbf{j}$ and $\mathbf{v}_s$ is nonlinear, given by Eq. (2.16) (see also (A2)), one can in principle use the following iteration method. As a first step, one can solve these equations in Ω with boundary conditions on $\partial\Omega$ corresponding to the limit $\varepsilon = 0$. That can be done by setting $A_{1\parallel} = A_{1\parallel}(\varepsilon = 0)$ (and all the other $A_{l\parallel,\perp}^m \equiv 0$), requiring continuity of the components H_η and H_φ at $\xi = \xi_0$, and also enforcing the condition on $\partial\Omega$, $\mathbf{j}\cdot\mathbf{n} = 0$. These boundary conditions for the magnetic field are not exactly the desired ones, since continuity of the ξ component cannot be demanded because the external field has been specified so that its ξ component vanishes at the boundary. The magnetic field outside the sample is simply obtained from Eq. (2.2a) with Φ given by (3.6). Inside one employs Eq. (2.4) to get the magnetic field from $\mathbf{v}_s$.

From the numerical solution in Ω, obtained using the overrelaxation method discussed in [19, 20] we can compute the magnetic moment by using (2.8), and the fields from the above approximate solution. The computed value, $\mathbf{m}^{(1)}$, the superscript (1) indicating the order of iteration, will be in general different from $m_0\hat{x}$: the computed magnetic moment is not the input value m_0. Hence, the actual problem has not been solved: the solution is not self-consistent. One can then imagine obtaining the correct solution from the following iteration process: Denote by $(A_{1\parallel})^{(1)}$, $(A_{1\perp})^{(1)}$ the values of these quantities obtained from Eqs. (3.8), Eq. (3.10) and the appropriate components of $\mathbf{m}^{(1)}$. Then use $(A_{1\parallel})^{(1)}$, $(A_{1\perp})^{(1)}$ in the computation of the exterior field, and use again this exterior field to solve Eq. (2.6), repeating the procedure described in the previous paragraph. The second iteration yields, e.g., $(A_{1\parallel})^{(2)}$, $(A_{1\perp})^{(2)}$ which in general would differ from $(A_{1\parallel})^{(1)}$ and $(A_{1\perp})^{(1)}$. Repeated iterations would give sequences $(A_{1\parallel})^{(1)}$, $(A_{1\parallel})^{(2)}$, $(A_{1\parallel})^{(3)}$, ... and $(A_{1\perp})^{(1)}$, $(A_{1\perp})^{(2)}$, $(A_{1\perp})^{(3)}$, ... converging to the desired values of $A_{1\parallel}$, $A_{1\perp}$, when the moment generated by the computed currents equals the input value. At that point, the magnetic moment will be known. The higher order As will not necessarily be known, but they do not contribute to $\mathbf{m}$. In practice such a procedure could be implemented first for the larger longitudinal component and then for the smaller transverse component.

B. *Perturbation Method To Compute* $\mathbf{m}$

The procedure described in IVA may be a lengthy and expensive process and it is for this reason that we develop, in this subsection, a procedure to bypass it. We compute

$m_\|$ (accurate to first order in ε) in a single iteration step, that is, a single pass through solving the equations inside the body as described above.

The surface integral (2.13), rather than (2.8) is the expression for $\mathbf{m}$ that is convenient for our purpose since as seen in subsection IIB, it divides $\mathbf{m}$ into two terms, $\mathbf{m}_1$ and $\mathbf{m}_2$, of different order in ε.

It follows from the considerations of Section II, and it is the basis of our perturbation method, that to obtain $\mathbf{m}$ correctly to $O(\varepsilon m_0)$ it is sufficient to compute $\mathbf{m}_2$ from fields (i.e., $\mathbf{H}$ or $\mathbf{v}_s$) accurate only to zeroth order. This is, as explained there, because a factor of ε explicitly scales out of the expression for $\mathbf{m}_2$. Now, since the internal fields obtained by solving Eq. (2.6) at the first iteration level (as described in the previous subsection, i.e., with $\varepsilon = 0$ boundary conditions) are already accurate to the zeroth order, one iteration is sufficient to evalute $\mathbf{m}_2$ at desired accuracy. The problem reduces, therefore, to that of correctly including the contribution $\mathbf{m}_1$ to first order in ε.

To illustrate how this is done, let us recall the general form of the analytic solution for the spheroid. As seen in Section III (Eq. (3.4)) it has the form of a multipole expansion with undetermined coefficients. Since the exact field $\mathbf{H}$ is continuous on $\partial\Omega$ we can insert this general form in the expression (2.13) for $\mathbf{m}_1$. Only the $l = 1$ terms, by virtue of (3.8) and (3.10), contribute to $\mathbf{m}$, so that $\mathbf{m}_1$ can be evaluated in terms of the unknown $\mathbf{m}$. Thus we have

$$\mathbf{m} = \mathbf{m}_1(\mathbf{m}) + \overline{\mathbf{m}}_2 + O(\varepsilon^2 m_0), \tag{4.1}$$

where we emphasize that $\mathbf{m}_1$ depends on the unknown $l = 1$ parameters, and where we introduce the overbar notation to denote quantities evaluated from the zero penetration limit external fields. Since terms of $O(\varepsilon^2 m_0)$ can be neglected, it is possible to interchange $\mathbf{m}_2$ and $\overline{\mathbf{m}}_2$ in the various expressions and we have done so. Expression (4.1) is an equation for the unknown $\mathbf{m}$.

To solve it in practice, consider the general form of Φ, Eq. (3.4) which indicates that Φ (or equivalently $\mathbf{H}$) can be separated into two parts: $\Phi = \Phi_a + \Phi_r$, due to the applied field and to the presence of the superconductor, respectively. We can then write the contribution of these parts as

$$\mathbf{m}_1(\mathbf{m}) = \mathbf{m}_1(\Phi_a) + \mathbf{m}_1(\Phi_r). \tag{4.2}$$

We now define p by $\mathbf{m}_1(\Phi_a) \equiv p\mathbf{m}_0$. Since $\mathbf{m}_0$ and $\mathbf{m}_1(\Phi_a)$ are now known, one can determine the constant p which depends on the shape of Ω, i.e. on the eccentricity. In the limit $\varepsilon = 0$, $\mathbf{m}_2 = 0$ and from Eq. (4.2) we have the identity

$$\mathbf{m}_0 = \overline{\mathbf{m}}_1 = p\mathbf{m}_0 + \mathbf{m}_0(1 - p). \tag{4.3}$$

For $\varepsilon \neq 0$, when the solution for Φ and $\mathbf{H}$ is given in terms of multipole expansion with unknown coefficients, $\mathbf{m}_1(\Phi_a)$ remains the same. The only difference in computing $\mathbf{m}_1$ is that the coefficients in the terms arising from Φ_r are now proportional to the correct, but still to be determined, value of the magnetic moment $\mathbf{m}$, slightly changed from the $\varepsilon = 0$ case. All the remaining higher multipoles ($l > 1$) of Φ, as mentioned in III, do not contribute to $\mathbf{m}$ and we have

$$\mathbf{m}_1(\Phi_r) = \mathbf{m}(1 - p). \tag{4.4}$$

Adding this to $\mathbf{m}_1(\Phi_a)$ we get

$$\mathbf{m}_1 = \mathbf{m} - p(\mathbf{m} - \mathbf{m}_0). \tag{4.5}$$

We can express Eq. (2.14) using (4.5) as

$$\mathbf{m} = \mathbf{m} - p(\mathbf{m} - \mathbf{m}_0) + \mathbf{m}_2, \tag{4.6}$$

so that we have the solution for $\mathbf{m}$ correct to $O(\varepsilon)$,

$$\mathbf{m} = \mathbf{m}_0 + \frac{1}{p}\mathbf{m}_2 \approx \mathbf{m}_0 + \frac{1}{p}\overline{\mathbf{m}}_2, \tag{4.7}$$

which determines all components of $\mathbf{m}$.

We illustrate this method using the textbook example of the isotropic, linear superconducting sphere in a uniform applied field $\mathbf{H}_a$, along the x-axis. In this case all the fields in Ω satisfy the vector Helmholtz equation

$$\nabla^2\mathbf{F} = \frac{1}{\lambda^2}\mathbf{F}, \tag{4.8}$$

where $\mathbf{F}$ can be $\mathbf{H}$, $\mathbf{j}$, $\mathbf{v}_s$. On the entire $\mathbf{R}^3\backslash\Omega$ region, Φ_r has a pure dipole form and $\mathbf{H}$ is given by taking the gradient of Eq. (3.11)

$$H_r = \left(H_a + \frac{2m}{r^3}\right)\sin\theta\cos\varphi, \tag{4.9a}$$

$$H_\theta = \left(H_a - \frac{m}{r^3}\right)\cos\theta\cos\varphi, \tag{4.9b}$$

$$H_\varphi = \left(-H_a + \frac{m}{r^3}\right)\sin\varphi, \tag{4.9c}$$

where r, θ, ϕ are spherical coordinates, and m a parameter to be determined. This is the general solution for any ε (not just 0), in the field outside; there is only a dipole term in addition to that due to applied field. However, even if there were higher spherical multipoles in the general solution, that would not affect the evaluation of m_1, since their contribution to $\mathbf{m}$ would vanish identically by symmetry. In the limit where the current does not penetrate into the superconductor, the magnetic moment is given by $m_0 = -\frac{1}{2}a^3 H_a$ (recall (3.12)). Performing the elementary integral for $\mathbf{m}_1$ in Eq. (2.14) we obtain

$$\mathbf{m}_1 = \tfrac{1}{3}\mathbf{m}_0 + \tfrac{2}{3}\mathbf{m} = \mathbf{m} - \tfrac{1}{3}(\mathbf{m} - \mathbf{m}_0), \tag{4.10}$$

Comparing with (4.5) we identify $p = \frac{1}{3}$ in this case and using Eq. (4.7)

$$\mathbf{m} = \mathbf{m}_0 + 3\overline{\mathbf{m}}_2. \tag{4.11}$$

To determine the unknown m to $O(\varepsilon)$ it remains to compute $\overline{\mathbf{m}}_2$ and substitute it in (4.11). Using the evaluation for $\overline{\mathbf{m}}_2$, with the boundary conditions taken in the $\varepsilon = 0$, from Appendix C we get the perturbation result for m

$$m = m_0(1 - 3\varepsilon), \tag{4.12}$$

where $\varepsilon = \lambda/a$. If we compare this to the expression for $m_\parallel$ given by Eq. (2.9a) we can read off $\alpha_\parallel = 3$. This is the correct value for a sphere to this order, as given in textbooks [9, 12]. This, using the perturbation method with approximate boundary conditions in the evaluation of m_2, we have obtained the correct value for m to first order in ε. It is also instructive to calculate m analytically, with internal fields evaluated from (2.6) and $\varepsilon = 0$ boundary conditions, Eq. (2.13). The calculation would yield m correct only to $O(m_0)$; the value of $\alpha_\parallel$ is not correct; one gets $\alpha_\parallel = 2$ instead of $\alpha_\parallel = 3$.

We return now to the oblate spheroid. In Ω we allow the full nonlinear relation between $\mathbf{j}$ and $\mathbf{v}_s$, given by Eq. (A2). The magnetic field in $\mathbf{R}^3\backslash\Omega$ that contributes to the computation of $\mathbf{m}$ is given in Appendix B3. We aim to obtain the appropriate perturbation equation (4.7) relating the unknown moment to $\overline{\mathbf{m}}_2$, the term computed from the numerical solution in Ω (using the first step in the iteration procedure, described in the previous subsection). To calculate the magnetic moment, we proceed as with the sphere example. We first evaluate the term $\mathbf{m}_1$ from Eq. (2.14), recalling Eqs. (3.7), (3.8), (3.10) and $\mathbf{n} = \hat{\xi}$. The integral, evaluated in spheroidal coordinates using (B6), is elementary and we give only the result. The corresponding perturbation equation for $\mathbf{m}$ is, from (4.7)

$$\mathbf{m} = \mathbf{m}_0 + \frac{1}{p(\xi_0)}\mathbf{m}_2, \tag{4.13}$$

or, writing its components explicitly

$$m_\parallel = m_0 + \frac{1}{p(\xi_0)} m_{2\parallel}, \tag{4.14a}$$

$$m_\perp = \frac{1}{p(\xi_0)} m_{2\perp}, \tag{4.14b}$$

with

$$p(\xi) = \tfrac{1}{4}(2 + \xi^2 - (1 + \xi^2)\xi \arctan(1/\xi)), \tag{4.15}$$

$p(\xi)$ is evaluated at the surface of the ellipsoid ($\xi = \xi_0$). As shown in Appendix B1, ξ_0 is related to the eccentricity of the spheroid. In the spherical limit when $\xi \to \infty$ we recover the sperical result, $p = \frac{1}{3}$, obtained earlier. Another interesting limit is that of a flat disk ($\xi \to 0$) where $p(\xi) = \frac{1}{2}$. As discussed previously, $m_\perp \to 0$ for $\tilde{\Lambda} \to 0$.

The above method applies not only to oblate spheroids, but to all geometries for which a general solution for Φ in $R^3\backslash\Omega$ as an expansion in terms of orthogonal functions, (only one of them being dipolar at large distances) can be written. Furthermore, the method can be extended, with one additional assumption, to a situation where the shape of Ω precludes an analytic solution for the outside fields even at $\varepsilon = 0$, and only a numerical solution, $\overline{\Phi}$, in that limit is available. We assume that, as in the analytic cases, the coordinate dependence of the terms in Φ which contribute to the dipole $\mathbf{m}$ remains the same, up to a multiplicative constant, for $\varepsilon = 0$ and $\varepsilon \neq 0$. This assumption requires that the shape of Ω produces no singularities in the fields. This might be a sufficient condition, but we know of no rigorous proof.

The magnetic field at large distances, $r \gg d$, has the form given in Eq. (3.11), m_0 is the magnetic moment for Ω, and all the higher multipoles can be neglected. We can again, as above (4.2) separate $\overline{\Phi} = \Phi_a + \overline{\Phi}_r$, where Φ_a is the applied field contribution. At $r \gg d$, $\overline{\Phi}_r$ is of dipolar form and the value of m_0 can be in principle numerically extracted either by using the left part of (4.3) or from the asymptotic form. For $\varepsilon \neq 0$ the potential Φ has asymptotically the same dipolar form as $\overline{\Phi}$, but the unknown dipolar coefficient $\mathbf{m}$ differs from $m_0\hat{x}$. One can then proceed as in the analytic case. Consider as an illustration, the computation of $m_\parallel$ to $O(\varepsilon)$. We can implement the method by writing the potential at $\varepsilon \neq 0$ in the form

$$\Phi(\varepsilon \neq 0) = \Phi_a + \frac{m_\parallel}{m_0}(\overline{\Phi}_r) + \Phi_{\mathrm{nd}}, \tag{4.16}$$

where Φ_{nd} is a possible contribution to higher order multipoles only. Eq. (4.16) merely expresses our assumptions in mathematical form. It can be better understood by recalling the discussion in Section III (and above in this Section) in particular the difference between $A_{1\parallel}(\varepsilon = 0)$ and $A_{1\parallel}$.

Since m_0 is known, one can use Φ_a to evaluate $\mathbf{m}_1(\Phi_a)$ (see (4.2)) and hence the quantity p through $m_1(\Phi_a) = pm_0$. From the distribution of $\mathbf{v}_s$ on $\partial\Omega$ we compute $\overline{m}_2$ and Eq. (4.7) gives the desired $m_\parallel$.

We see therefore that our method has considerable generality and our results can be summarized in terms of the following theorem, the validity of which follows from the analysis in this section and the decomposition of $\mathbf{m}$ in IIB.

THEOREM 1. *Let us assume that:*

(a) *There exist a small parameter* $\varepsilon \ll 1$ *and we consider Eq.* (2.6) *in* Ω *that allows a sufficiently accurate solution in* $\mathbf{R}^3\backslash\Omega$ *for* (2.2b) *with trivial Neumann boundary conditions on* $\partial\Omega$, *and at infinity* $-\nabla\Phi = \mathbf{H}_a$, *which satisfies the assumption discussed in connection with* (4.16).

(b) $\mathbf{H}$ *in the interior of* Ω *decreases with the distance from* $\partial\Omega$ *not slower than exponential dependence given by a characteristic length* $\ll$ *typical size of* Ω.

Then the following statements are true:

1. *It is possible to write* $\mathbf{m} = \mathbf{m}_1 + \mathbf{m}_2$ *as given by* (2.14) *where* m_1 is $O(m_0)$ *and* m_2 *is* $O(\varepsilon m_0)$.
2. *To obtain* $\mathbf{m}$ *from Eq.* (4.7) *accurate to* $O(\varepsilon m_0)$ *it is sufficient to calculate the leading contribution to the term* $\mathbf{m}_2$, *the error in determining* $\mathbf{m}$ *being of* $O(\varepsilon^2 m_0)$.

This perturbation method can be applied outside the field of superconductivity. For example, it is well known [1] that an ordinary conductor in a high frequency, harmonic applied magnetic field (the frequency should satisfy quasi-static condition $\omega \ll c/d$) behaves like a superconductor in a constant field. It is then possible to identify the small parameter, $\varepsilon \ll 1$ as the ratio of skin depth, δ_s, the typical length scale for field penetration in the conductor and the characteristic geometrical dimension, d. The computation of the magnetic field distribution is then achieved by solving the corresponding steady-state problem for a superconductor of the same shape, and $\mathbf{m}$ can be obtained using Eq. (4.7).

V. NUMERICAL CONSIDERATIONS

A. *Dimensionless Form of Equations on* Ω

In performing the calculations and describing the results, it is convenient to introduce dimensionless quantities. We recall that Ω is a flat spheroid and with the magnetic field applied in the $x - y$ $(a - b)$ plane, most of the current will flow parallel to the $a - b$ plane and its decay will be governed by λ_{ab}. It is therefore convenient to measure the length in the units of λ_{ab}. We then define dimensionless fields $\mathbf{V}$, $\mathbf{J}$, and $\mathscr{H}$:

$$\mathbf{V} = \frac{\mathbf{v}_s}{v_c}, \quad \mathscr{H} = \frac{\mathbf{H}}{H_0}, \quad \mathbf{J} = \frac{cH_0}{4\pi\lambda_{ab}}\mathbf{j}, \tag{5.1}$$

where $v_c = \Delta_0/v_f$ is the critical velocity (discussed in Appendix A), Δ_0 is the amplitude of the order parameter, defined in Appendix A, and we have introduced a characteristic magnetic field H_0 as

$$H_0 = \frac{\phi_0}{\pi^2\lambda_{ab}\xi_{ab}}, \tag{5.2}$$

where $\phi_0 = \pi c\hbar/e$ is the flux quantum and $\xi_{ab} = v_f/(\pi\Delta_0)$ is the in-plane superconducting coherence length (not to be confused with ξ, the spheroidal coordinate). The definition (5.2) involves precisely the same numerical factors as that used in [4, 6]. The required equations are easily rewritten in terms of these quantities. Equation (2.6), using the relation between $\mathbf{j}$ and $\mathbf{v}_s$ given by (A2), then becomes

$$\begin{aligned}(\nabla\times\nabla\times\mathbf{V})_{x',y'} &= -V_{x',y'}(1 - t_1|V_{x',y'}|)\\ &\equiv -V_{x',y'} + N_{x',y'}, \end{aligned}\tag{5.3a}$$

$$\begin{aligned}(\delta\nabla\times\nabla\times\mathbf{V})_z &= -V_z\left(1 - t_2\frac{V_{x'}^2 + V_{y'}^2}{|V_{x'}| + |V_{y'}|}\right)\\ &\equiv -V_z + N_z, \end{aligned}\tag{5.3b}$$

where $\delta = (\lambda_c/\lambda_{ab})^2 = m_c/m_{ab}$ and we define $N_{x'}, N_{y'}, N_z$ as the terms nonlinear in the velocity. The equations are written in terms of the primed coordinates and the derivatives are with respect to the dimensionless length measured in units of λ_{ab}.

Before discretizing Eqs. (5.3) we transform them to oblate spheroidal coordinates. We start by writing these equations in the unprimed (x, y, z) coordinate system where, we recall, the x-axis lies along the applied field. The linear part of the equations looks identical in primed or unprimed coordinates and we only need to carefully transform $N_{x',y',z}$ to N_x, N_y and N_z terms nonlinear in the velocity along the unit vectors $\hat{x}$, $\hat{y}$, and $\hat{z}$, respectively. We have

$$N_x = t_1(V_{x'}|V_{x'}|\cos\Psi + V_{y'}|V_{y'}|\sin\Psi), \tag{5.4a}$$

$$N_y = -t_1(V_{x'}|V_{x'}|\sin\Psi - V_{y'}|V_{y'}|\cos\Psi), \tag{5.4b}$$

$$N_z = t_2 V_z\frac{V_{x'}^2 + V_{y'}^2}{|V_{x'}| + |V_{y'}|}, \tag{5.4c}$$

where $V_{x'} = V_x\cos\Psi - V_y\sin\Psi$, $V_{y'} = V_x\sin\Psi + V_y\cos\Psi$ and $V_{z'} = V_z$. Or, if we express the components of velocity in spheroidal coordinates

$$V_{x'} = \cos(\varphi + \Psi)(aV_\xi + dV_\eta) - \sin(\varphi + \Psi)V_\varphi, \quad (5.5a)$$

$$V_{y'} = \sin(\varphi + \Psi)(aV_\xi + dV_\eta) + \cos(\varphi + \Psi)V_\varphi, \quad (5.5b)$$

$$V_z = -dV_\xi + aV_\eta, \quad (5.5c)$$

where $a = \xi(1 - \eta^2)^{1/2}/(\xi^2 + \eta^2)$ and $d = -(1 + \xi^2)^{1/2}\eta/(\xi^2 + \eta^2)$. We can now write the nonlinear part (from equation (2.6) and (5.4)) along each spheroidal coordinate. For example, along $\hat{\xi}$ we get

$$N_\xi = a(\cos\varphi N_x + \sin\varphi N_y) - dN_z. \quad (5.6)$$

$N_{x,y,z}$ are entirely expressed in terms of spheroidal components as shown above. In an analogous way we can obtain the remaining nonlinear parts $N_{\eta,\varphi}$.

Using Eqs. (3.2) we transform the inverse of the penetration depth tensor given in Cartesian coordinates by a diagonal tensor with components $(\lambda_{ab}^{-2}, \lambda_{ab}^{-2}, \lambda_c^{-2})$, (recall Eq. (2.17)) to spheroidal coordinates:

$$\tilde{\Lambda}^{-1} = \lambda_{ab}^{-2}\begin{bmatrix} \rho_1 & \rho_2 & 0 \\ \rho_2 & \rho_3 & 0 \\ 0 & 0 & 1 \end{bmatrix}$$

where $\rho_{1,2,3}$ are defined by

$$\rho_1 = \frac{\xi^2(1 - \eta^2) + \delta^{-1}(1 + \xi^2)\eta^2}{\xi^2 + \eta^2}, \quad (5.8a)$$

$$\rho_2 = -\frac{(1 - \delta^{-1})\xi(1 + \xi^2)^{1/2}\eta(1 - \eta^2)^{1/2}}{\xi^2 + \eta^2}, \quad (5.8b)$$

$$\rho_3 = \frac{\delta^{-1}\xi^2(1 - \eta^2) + (1 + \xi^2)\eta^2}{\xi^2 + \eta^2}. \quad (5.8c)$$

The resulting form of the dimensionless equations in spheroidal coordinates (which we will solve numerically) is

$$f^2(\nabla \times \nabla \times \mathbf{V})_\xi = -f^2((\rho_1 V_\xi + \rho_2 V_\eta) - N_\xi), \quad (5.9a)$$

$$f^2(\nabla \times \nabla \times \mathbf{V})_\eta = -f^2((\rho_2 V_\xi + \rho_3 V_\eta) - N_\eta), \quad (5.9b)$$

$$f^2(\nabla \times \nabla \times \mathbf{V})_\varphi = -f^2(V_\varphi - N_\varphi). \quad (5.9c)$$

Expressions for the differential operator $f^2\nabla \times \nabla \times \mathbf{V}$ in spheroidal coordinates are included in Appendix B2. Equations (5.9) have to supplemented with appropriate boundary conditions, as discussed in Section II. The boundary condition at infinity is satisfied by the use of the analytic solution for $\mathbf{R}^3\backslash\Omega$. Since $\lambda_{ab} \ll C$ we can put $\mathbf{V} \equiv 0$ at $\xi = 0$, as all the fields vanish deep inside the sample. Continuity of the $\mathscr{H}$ field on $\partial\Omega$ is achieved through

$$\nabla \times \mathbf{V} = \mathscr{H}|_{\xi=\xi_0}, \quad (5.10)$$

where the right hand side is the external dimensionless field at the surface of the ellipsoid. The remaining boundary condition $\mathbf{J}\cdot\mathbf{n} \equiv J_\xi = 0$ on $\partial\Omega$ is generally nonlinear and readily enforced by observing that the RHS of Eq. (5.9a) is $\propto J_\xi$.

B. *Computational Grid and Discrete Variables*

The implementation of the perturbation method from Section IV is not restricted to a particular algorithm for solving the relevant equations in Ω. In the remaining part of this section we outline as an example one suitable algorithm using a modification of the Gauss–Seidel relaxation method. We first discuss the discretization of the complete nonlinear, three-dimensional (3D) problem. It is then possible to consider, as a special case, the two-variable discretization of the linear problem were the φ dependence is known analytically. The numerical solution to such a problem is then used as the initial guess for the relaxation method of the complete 3D problem.

Eqs. (5.9) or their counterparts (2.6) and (A2), have definite parity: v_x, v_y are even and v_z is odd in z. It is therefore sufficient to consider only the upper, *positive* z (Ω_+), or the lower, *negative* z (Ω_-) half of Ω and extend by parity the obtained solution to the whole Ω. The computational domain G is obtained by parameterizing the physical domain Ω_- using oblate spheroidal coordinates (ξ, η, φ). We consider a uniform grid on G with mesh widths h_ξ, h_η and h_φ. The choice of a grid uniformly spaced in variable η, generates denser grid points corresponding to the part of Ω_- (the $\eta \approx 0$ region) with higher curvature and greater field variation. An arbitrary grid point on G is given by (ξ_i, η_j, φ_k) or just (i, j, k) for brevity

$$\mathbf{x}_{i,j,k} = \xi_i\hat{\xi} + \eta_j\hat{\eta} + \varphi_k\hat{\varphi}, \quad (5.11)$$

where the grid coordinates are given by

$$\xi_i = ih_\xi, \eta_j = -1 + (\tfrac{1}{2} + j)h_\eta, \varphi_k = -\pi + kh_\varphi, \quad (5.12)$$

and the indices run through values $i = 0, ..., n_\xi$, $j = 0, ..., n_\eta$ and $k = 0, ..., n_\varphi$. Mesh widths are given by $h_\xi = \xi_0/n_\xi$, $h_\eta = 2/(2n_\eta + 1)$ and $h_\varphi = 2\pi/n_\varphi$.

The discrete variables are denoted by the same symbol as their continuous counterparts, for example, $\mathbf{V}_{\xi;i,j,k}$ represents $\mathbf{V}_\xi$ at the grid point (ξ_i, η_j, φ_k). The discretized approximations of derivatives used have second order accuracy in the mesh widths. We will use the letter D to represent the discretized approximation, upper indices 0, $+$, $-$ denote the central, forward and, backward approximation respectively, and the lower indices denote the corresponding variables of differentiation. For example,

$D^{0+}_{\xi\eta}$ denotes the mixed differentiation with respect to ξ and η, where the central difference formula is used in ξ and the forward difference formula in η variable. For the interior grid points we only use the central difference formula for all the derivatives and omit the upper indices. We also use central differences for derivatives at all the grid points on ∂G that do not require introduction of fictitious grid points $\notin G$. For example, in computing D^0_ξ at (n_ξ, j, k) we would need to use a grid point at $i = n_\xi + 1 \notin G$, we avoid that by using a backward difference D^-_ξ at (n_ξ, j, k). Similarly we employ forward differences were necessary.

C. *Implementation of Boundary Conditions and Equations on G*

The grid boundary, ∂G, consists of six two-dimensional planar surfaces with grid points described by $(0, j, k)$, (n_ξ, j, k), $(i, 0, k)$, (i, n_η, k), $(i, j, 0)$, and (i, j, n_φ).

On the surface $\xi = 0$, $(0, j, k)$, which corresponds to the equatorial ($z = 0$) disk in Ω with radius equal to the focal length f, we impose trivial Dirichlet boundary conditions. As we have discussed in Section II, this follows from the requirement that deep inside Ω all fields should vanish. This eliminates possible difficulties from the singularities of the various differential operators at $\xi = 0$. Any remaining singularities of the equations on G would come from points with coordinates $\eta = 0$ and $\eta = \pm 1$. On the surface $\eta = 0$ $(i, j = n_\eta, k)$, corresponding to part of the $z = 0$ plane, we have from the known parity of $\mathbf{V}$:

$$V_{\xi,\varphi} = 0\big|_{\eta=0}, \tag{5.13a}$$

$$\partial_\eta V_\eta = 0\big|_{\eta=0}. \tag{5.13b}$$

We implement Eq. (5.13b) as $D^-_\eta V_{\eta;i,j=n_\eta,k} = 0$

$$D^-_\eta V_{\eta;i,j,k} = \frac{1}{2h_\eta}(3V_{\eta;i,j,k} - 4V_{\eta;i,j-1,k} + V_{\eta;i,j-2,k}), \tag{5.14}$$

and in the iterative solution we write down explicitly $V_{\eta;i,j,k}$ from this expression. The remaining region on G that could result in singularities of the differential operators is at $\eta = -1$, which corresponds to a line through the "south pole" and the origin of Ω, i.e., a segment starting at the origin and ending at a point with Cartesian coordinates $(0, 0, z)$. The choice of grid given in Eq. (5.12) excludes this segment, the closest point on the grid in $h_\eta/2$ away. The numerical solution for $\mathbf{V}$ in the vicinity of $\eta = -1$ is well behaved (as it is for the linearized equations in the geometries that permit an analytic solution in Ω). It is therefore possible to extrapolate the obtained numerical solution to $\eta = -1$. At the grid boundary surface $(i, j = 0, k)$ we use the forward difference formula for the derivatives with respect to η, D^+_η is obtained analogous to Eq. (5.14) by replacing h_η with $-h_\eta$ and the indices $j - 1$, $j - 2$ by $j + 1$ and $j + 2$ respectively. The second derivative $D^{++}_{\eta\eta}$ is taken as:

$$D^{++}_{\eta\eta}F_{i,j,k} = \frac{1}{h^2_\eta}(-F_{i,j+3,k} + 4F_{i,j+2,k} - 5F_{i,j+1,k} + 2F_{i,j,k}), \tag{5.15}$$

where F represents any component of a vector field. We can obtain similar formulae for $D^{0+}_{\xi\eta}$ and $D^{+0}_{\eta\varphi}$. At the surface boundary $(i, j, k = 0)$, where $\varphi = -\pi$, we proceed in an analogous way, the derivatives with respect to φ are expressed with forward differences. The other part of ∂G with $\varphi = \text{const}$, i.e., $(i, j, k = n_\varphi)$ corresponds to the same boundary surface ($\varphi = -\pi$) and we can impose the simple periodic boundary conditions

$$F_{i,j,n_\varphi} = F_{i,j,0}. \tag{5.16}$$

On the remaining part of ∂G, the surface $(i = n_\xi, j, k)$ at $\xi = \xi_0$, we impose continuity (as discussed in section IV) of the η and φ components of $\mathscr{H}$. From Eq. (5.10) we can express $V_{\eta;i,j,k}$ and $V_{\varphi;i,j,k}$ respectively to obtain their updated values in each step of the relaxation procedure. The equation for $V_{\xi;i,j,k}$ is obtained from $\mathbf{J}\cdot\mathbf{n} = 0$ by setting the RHS of Eq. (5.9a) to zero

$$\rho_1 V_\xi + \rho_2 V_\eta - N_\xi = 0. \tag{5.17}$$

In the relaxation procedure, the nonlinear term N_ξ is included using Picard's method [21], the value of N_ξ is taken from the previous iteration. If we denote by an upper index n the number of the iteration (in the relaxation procedure), the nonlinear boundary condition can be implemented as

$$V^{n+1}_\xi = -\frac{\rho_2}{\rho_1}V^{n+1}_\eta + \frac{1}{\rho_1}N^n_\xi. \tag{5.18}$$

The nonlinear and nonanalytic terms can be simply included by using Picard's method. In addition to the nonlinear boundary condition (5.18) we shall also use Picard's method to include the nonlinearities stemming from Eq. (5.9).

For the grid points $\notin \partial G$ it is possible to use central differences. In the LHS of Eq. (5.9), given explicitly in Appendix C, we replace each partial derivative by the appropriate central difference, D.

D. *Modified Gauss-Seidel Relaxation*

The solution to the nonlinear, 3D problem using the relaxation method consists of two steps. The first is obtaining a good initial guess using the numerical solution to the linear equations given by Eqs. (2.6) and (2.17). The φ dependence is then known and it can be separated out. The method of successive overrelaxation can be applied to the resulting two-variable problem in the coordinates ξ and η. The boundary conditions on the continuity of $\mathscr{H}$, as discussed in the previous subsection, are implemented: the magnetic field outside is taken in the $\varepsilon = 0$ limit ($A_{1\|} = A_{1\|}(0)$). In the relaxation procedure each component of $\mathbf{V}$ is expressed in terms of the corresponding component of the linearized ($N_{\xi,\eta,\varphi} = 0$), two-dimensional form of Eq. (5.9) so that the resulting matrix equation is diagonally dominant [22]. For a detailed discussion of the method see [19, 20]. The numerical solution, the distribution of $V(\xi_i, \eta_j)$, is supplemented with the known φ dependence and $m_\|$ is calculated using the perturbation method.

The second part of the algorithm is a modification of the Gauss–Seidel (the overrelaxation parameter, $\omega = 1$) method for the full 3D problem. The previously obtained solution for the linearized equations is the initial guess for $V_{i,j,k}$, and the value $m_\|$ i.e., the corresponding $A_{1\|}$, is used in the expression for the $\mathscr{H}$ outside. If we denote the linear part of Eq. (5.9) as $\mathbf{L}(\mathbf{V})$ and the nonlinear part as $\mathbf{N}(\mathbf{V})$ the relaxation procedure can be described symbolically as:

$$\mathbf{L}(\mathbf{V}^{(n+1)}) = \mathbf{N}(\mathbf{V}^{(n)}), \quad n = 1, 2, \ldots \tag{5.19}$$

After completion of each relaxation step we update the old values, $\mathbf{V}^{(n)}$, at each grid point as $\mathbf{N}(\mathbf{V}^{(n)}) = \mathbf{N}(\mathbf{V}^{(n+1)})$. As done with the boundary condition from Eq. (5.18) we use Picard's method to include the nonlinear terms which are also nondifferentiable. The numerical solution for the linearized equations is a very good initial guess for the full problem, since the nonlinear terms are small, which compensates for the relatively slow convergence of Picard's method.

VI. NUMERICAL TESTS

For our computations we used the Cray C90 of the Minnesota Supercomputer Institute. We first tested the computer code on the example of the linear, isotropic sphere with applied field along the x axis, where the analytic solution is known. The spherical geometry was realized as the spherical limit of the spheroid. We used $\xi_0 = 1000$ and $f = 0.1$, so that the radius of sphere was $a \to f\xi_0 = 100$ (in units of λ), the corresponding $\varepsilon = \lambda/a = 10^{-2}$ and the ratio of the spheroidal semi-axes is $A/C = 100.005/100$. We used the two-variable version of the code in the variables ξ and η. The computational grid spanned a spherical shell of thickness 7 (λ), and because fields decay exponentially away from the surface, we imposed trivial Dirichlet conditions at $\xi = 930$. We used $n_\xi = 200$ and $n_\eta = 50$ for the number of grid points. To test the convergence of the relaxation algorithm, we tried the very poor initial guess of zero fields everywhere on G. The boundary conditions were taken in the $\varepsilon = 0$ limit, that is $A_{1\|} = A_{1\|}(\varepsilon = 0)$ from Eq. (3.7). The overrelaxation parameter was $\omega = 1.8$ and after 1000 relaxation steps (43 sec of CPU time) we obtained $\mathbf{m}$ using Eq. (2.14) and the perturbation method with Eq. (4.11). In the term $\mathbf{m}_2$ the distribution of V_η, V_φ at $\xi = \xi_0$ (from the numerical solution on G) was extended by parity to the entire $\partial\Omega$ and supplemented with the known φ dependence. Thus, integration over φ was performed analytically and that with respect to η, numerically. The extracted constant (from Eq. (4.11)) was $\alpha_\| = 3.1$, within 3% of the analytically obtained value of 3 from Eq. (4.12). The use of a conventional procedure to compute m would require repeating the whole iteration procedure to get an improved value for $\alpha_\|$, as we have in principle described in IVB.

We also verified that the numerical solution for the full three-variable problem in this geometry and exact boundary conditions, has the correct form. The angular dependence of the solution was J_η, $V_n \propto \eta \sin\varphi$ and J_φ, $V_\varphi \propto (1 - \eta^2)^{1/2} \cos\varphi$ which in the spherical limit $\eta \to \cos\theta$ corresponds to the analytical solution for a sphere. The numerical solution, for the range of grids considered, was accurate between three and four significant figures for every grid point where $\mathbf{J}(\mathbf{V})$ was numerically significant.

For the physical results related to the nonlinear response of an oblate spheroid we refer to [6], and discuss here only some aspects not covered there, that illustrate the numerics. Analysis of the transverse magnetic moment shows that [6]

$$m_\perp \propto \frac{H_a}{H_0} H_a F(\Psi), \tag{6.1}$$

from which we infer that $\alpha_\perp \propto H_a/H_0 F(\Psi)$, where $F(\Psi)$ is the angular dependence on Ψ which has [6] period $\pi/2$. We will give results for $\Psi = \pi/8$, approximately the maximum of F. The longitudinal moment, due to field penetration, differs from m_0 and it can be characterized, as we have shown earlier, by the parameter $\alpha_\|$. This parameter includes contributions from the linear part of $\mathbf{j}(\mathbf{V})$, independent of H_a, and from the nonlinear part, dependent both on H_a/H_0 and on Ψ.

We consider an oblate spheroid with $\xi_0 = 0.144338$ ($A/C = 7$) at $H_a/H_0 = 0.1$ (in the experimentally relevant range) and $\Psi = \pi/8$. For $f = 1000$ (in units of λ_{ab}, defined in IIC and VA) we have used $n_\xi = 550$, $n_\eta = 50$ and $n_\varphi = 30$. The results for $\alpha_\|$ and $\alpha_\perp$ are given as a function of the material parameter $\delta = (\lambda_c/\lambda_{ab})^2$ in Table I. For fixed ξ_0 (fixed shape), we have considered various sizes of spheroid (different f), changing $\varepsilon \equiv \lambda_{ab}/C \ll 1$ by a factor

TABLE I

The Parameters $\alpha_{\|}, \alpha_{\perp}$ Which Determine the Magnetic Moment for $\varepsilon \neq 0$ (see Eq. (2.9), Given as Functions of the Material Parameter $\delta = (\lambda_c/\lambda_{ab})^2$, Computed for an Oblate Spheroid with $A/C = 7$ at a Field $H_a/H_0 = 0.1$

$\delta = (\lambda_c/\lambda_{ab})^2$	$\alpha_{\|}$	$10^3\ \alpha_{\perp}$
16	1.9	3.8
25	2.1	3.6
36	2.2	3.3
50	2.3	3.1

of four (at fixed λ_{ab}, λ_c) and verified that $\alpha_{\|}$, $\alpha_{\perp}$ are size independent within numerical accuracy.

In the next two figures we display some of the numerical results for the field distributions calculated under the same conditions and with the same parameter values as in the previous paragraph. In Fig. 3, we show results for the current at surface of the spheroid, ($\xi = \xi_0$). The components $J_{\xi,\eta}(\xi_0, \eta, \varphi)$, at the fixed azimuthal angle $\varphi = 48°$, are shown as functions of η. For comparison we recall there also the corresponding angular behavior for a sphere, as given earlier in this Section. In Fig. 4 we show some results for the magnetic field as it penetrates into the sample. We plot the two components $\mathscr{H}_{\eta,\varphi}(\xi, \eta, \varphi)$ as functions of $\xi_0 - \xi$ at constant $\varphi = 0°$, $\eta = -0.693$, (see Fig. 2). The plot illustrates the difference between the components of the field arising purely from the linear equations and those which are due to the nonlinear effects. The component $\mathscr{H}_\eta$ (at $\varphi = 0°$) is very predominantly "linear," and displays exponential-like behavior. The other component plotted, $\mathscr{H}_\varphi$, vanishes in the linear case (at $\varphi = 0°$), and it arises solely from the nonlinear effects. This behavior is far from being an exponential; its derivative changes sign, for the same physical reasons as the nonlinear current does, as discussed in [6].

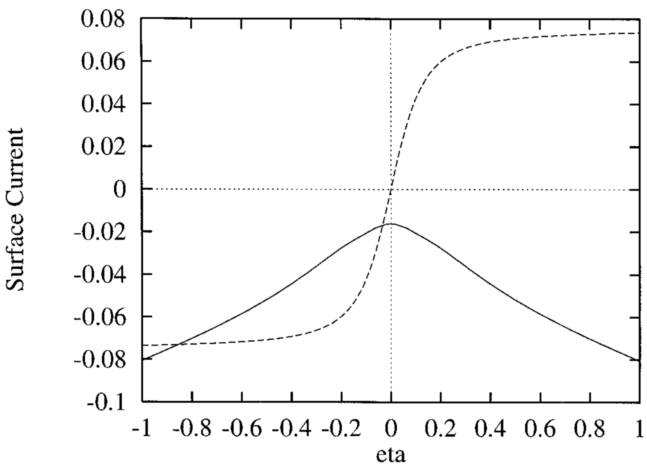

FIG. 3. The spheroidal components of the dimensionless current (see (5.1)) at the surface of the spheroid ($\xi = \xi_0$). The quantities plotted are $J_\eta(\xi_0, \eta, \varphi = 48°)$ (solid line) and $J_\varphi(\xi_0, \eta, \varphi = 48°)$ (dashed line). We have used $H_a/H_0 = 0.1$, $A/C = 7$, $\Psi = \pi/8$, $\delta = 16$.

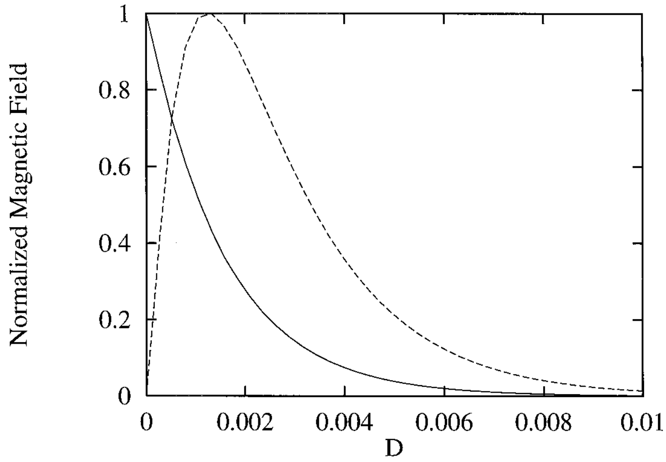

FIG. 4. Illustration of the nonlinear effects on the magnetic field. The solid line is the component $\mathscr{H}_\eta(\xi, \eta = -0.693, \varphi = 0°)$, which is very predominantly "linear," normalized to its maximum value, while the dashed line is $\mathscr{H}_\varphi(\xi, \eta = -0.693, \varphi = 0°)$, which arises solely from nonlinear effects, also normalized to its own, much smaller, maximum value. Both components are plotted as functions of $D \equiv \xi_0 - \xi$. The non-exponential behavior of the dashed line is a signature of its nonlinear character. All parameters used are as in the previous figure.

VII. CONCLUSIONS AND FUTURE WORK

In this paper, as the main result, we have presented a perturbation method to compute the magnetic moment of a bulk nonlinear and anisotropic superconductor. This method could be implemented in conjunction with various algorithms for solving boundary value problems in electrodynamics. Suitable generalizations would certainly increase the range of its applicability from that discussed in this paper. Obvious examples include considering in detail other shapes of Ω and computing higher order multipoles. We have showed that our method increases the accuracy of computation while very significantly reducing the required computational work.

In this paper the numerical example of an oblate spheroidal geometry was discussed in detail to illustrate the perturbation method and also to give guidelines for possible improvements. The numerical algorithm which was employed for solving the nonlinear Maxwell–London equations provided more than sufficient accuracy, as seen from experimental considerations: the uncertainty of the input experimental parameters significantly exceeds the accuracy of the results obtained. For our computations we have used Cray C90 and memory requirements were not the limiting factor. It is however possible to make various improvements to the numerical algorithm. One could consider nonuniformly spaced grid points along the ξ coordinate, denser close to the $\xi = \xi_0$, in order to reduce the overall number of grid points. It might also be advantageous to replace the Gauss–Seidel relaxation on G by some other method, such as GMRES [23] or one of the various multigrid algorithms [19]. In future work we will consider some of these improvements and investigate possible generalizations of the perturbation method presented in this paper.

APPENDIX A

The Nonlinear Relation $\mathbf{j}(\mathbf{v}_s)$

In order to express $\mathbf{j}(\mathbf{v}_s)$ from Eq. (2.16), we introduce two coordinate systems: $x - y$, fixed in space such that the applied field is along the x-axis, and $x' - y'$ which is fixed to the crystal. We consider an order parameter of the so called d-wave form:

$$\Delta = \Delta_0 \sin(2\phi), \tag{A1}$$

where ϕ is the azimuthal angle referred to a node and Δ_0 the gap amplitude. It has been shown [6] that in the field range of experimental interest and with suitable assumptions for the Fermi surface, Eq. (2.16) can be rewritten, at sufficiently low temperatures as

$$j_{x',y'} = -e\rho_{ab} v_{x',y'} \left(1 - \frac{t_1}{v_c}\left|v_{x',y'}\right|\right), \tag{A2a}$$

$$j_z = -e\rho_c v_z \left(1 - \frac{t_2}{v_c}\frac{v_{x'}^2 + v_{y'}^2}{\left|v_{x'}\right| + \left|v_{y'}\right|}\right), \tag{A2b}$$

where t_1 and t_2 are constants, $t_1 = (9\pi/64)$, $t_2 = (3\pi/32)$. The critical velocity is $v_c = \Delta_0/v_f$. We define here $\rho_{ab} = (c^2/(4\pi e^2))\lambda_{ab}^{-2}$ and $\rho_c = \rho_{ab}(\lambda_{ab}^2/\lambda_c^2)$.

APPENDIX B

Quantities in Spheroidal Coordinates

1. *Magnetic Moment*

We show here that the expression for the longitudinal magnetic moment for an oblate spheroid, given by Eq. (3.8), is equivalent to the standard result expressed in terms of the demagnetization factors. For a field applied along the x axis, in the limit $\tilde{\Lambda} = 0$, we have [1]

$$m_{0\|} \equiv m_{0x} = -\frac{H_a V}{4\pi(1 - n_x)}, \tag{B1}$$

where V is the volume of a spheroid and

$$n_x = -\frac{1}{2} - \frac{1 + e^2}{2e^3}(e - \arctan(e)) \tag{B2}$$

is the appropriate demagnetization factor. The eccentricity is given by $e = [A^2/C^2 - 1]^{1/2} = 1/\xi_0$. In terms of spheroidal coordinates we have $A = f(1 + \xi_0^2)^{1/2}$, $C = f\xi_0$ and $V = (4\pi/3)f^3(1 + \xi_0^2)\xi_0$. Including these expressions in Eq. (B1) we get

$$m_\| = -\frac{2}{3} f^3 H_a \frac{\xi_0}{1 + 1/(1 + \xi_0^2) - \xi_0 \arctan(1/\xi_0)} \tag{B3}$$

and we recover $m_\| = \frac{2}{3} f^3 A_{1\|}$.

2. *Integral and Differential Operators*

The metric coefficients in oblate spheroidal coordinates are given by [17]:

$$g_{11} = f^2 \frac{\xi^2 + \eta^2}{1 + \xi^2}, \tag{B4a}$$

$$g_{22} = f^2 \frac{\xi^2 + \eta^2}{1 - \eta^2}, \tag{B4b}$$

$$g_{33} = f^2(1 + \xi^2)(1 - \eta^2). \tag{B4c}$$

One can then calculate the appropriate elements of integration and differential operators. For example,

$$\int_{\partial\Omega} dS = \int_{-1}^{1} d\eta \int_0^{2\pi} d\varphi f^2 (1 + \xi^2)^{1/2} (\xi^2 + \eta^2)^{1/2}, \tag{B5}$$

$$\int_\Omega d\Omega = \int_0^{\xi_0} d\xi \int_{-1}^{1} d\eta \int_0^{2\pi} d\varphi f^3 (\xi^2 + \eta^2). \tag{B6}$$

ξ_0 corresponds to the value of ξ at the boundary $\partial\Omega$. The gradient is

$$\begin{aligned} \nabla = {} & \frac{(1 + \xi^2)^{1/2}}{f(\xi^2 + \eta^2)^{1/2}} \hat{\xi}\partial_\xi + \frac{(1 - \eta^2)^{1/2}}{f(\xi^2 + \eta^2)^{1/2}} \hat{\eta}\partial_\eta \\ & + \frac{1}{f(1 + \xi^2)^{1/2}(1 - \eta^2)^{1/2}} \hat{\varphi}\partial_\varphi. \end{aligned} \tag{B7}$$

To solve equations (2.6) the expression $\nabla \times \nabla \times \mathbf{v}$ should be transformed to oblate spheroidal coordinates:

$$\begin{aligned} f^2(\nabla \times \nabla \times \mathbf{v})_\xi = {} & a_0 \partial_{\eta\eta} v_\xi + a_1 \partial_\eta v_\xi + a_2 \partial_{\varphi\varphi} v_\xi + a_3 v_\xi + a_4 \partial_{\xi\eta} v_\eta \\ & + a_5 \partial_\xi v_\eta + a_6 \partial_\eta v_\eta + a_7 v_\eta \\ & + a_8 \partial_{\xi\varphi} v_\varphi + a_9 \partial_\varphi v_\varphi, \end{aligned} \tag{B8}$$

$$\begin{aligned} f^2(\nabla \times \nabla \times \mathbf{v})_\eta = {} & b_0 \partial_{\xi\eta} v_\xi + b_1 \partial_\xi v_\xi + b_2 \partial_\eta v_\xi + b_3 v_\xi + b_4 \partial_{\xi\xi} v_\eta \\ & + b_5 \partial_\xi v_\eta + b_6 \partial_{\varphi\varphi} v_\eta + b_7 v_\eta \\ & + b_8 \partial_{\eta\varphi} v_\varphi + b_9 \partial_\varphi v_\varphi, \end{aligned} \tag{B9}$$

$$f^2(\nabla \times \nabla \times \mathbf{v})_\varphi = p_0\partial_{\xi\varphi}v_\xi + p_1\partial_\varphi v_\xi + p_2\partial_{\eta\varphi}v_\eta + p_3\partial_\varphi v_\eta + p_4\partial_{\xi\xi}v_\varphi + p_5\partial_{\eta\eta}v_\varphi + p_6\partial_\xi v_\varphi + p_7\partial_\eta v_\varphi + p_8 v_\varphi. \tag{B10}$$

We recall that f is the focal length scale factor. The coefficients a_i, b_i, p_i are given by (using the abbreviations $u \equiv (1+\xi^2)^{1/2}$, $s \equiv (1-\eta^2)^{1/2}$, $w \equiv (\xi^2+\eta^2)^{1/2}$):

$$\begin{aligned}
&a_0 = -\frac{s}{u}\, a_4 = \frac{s}{u}\, b_0 = -\frac{s^2}{u^2}\, b_4 = \frac{s^2}{u^2}\, p_4 = p_5 = -\frac{s^2}{w^2},\\
&a_1 = -\frac{\eta}{\xi}\, b_5 = \frac{\eta}{\xi}\, p_6 = -p_7 = -\frac{2\eta}{w^2},\\
&a_2 = -\frac{w}{\xi s}\, a_9 = b_6 = -\frac{w}{u\eta} - p_8 = -\frac{1}{u^2 s^2},\\
&a_3 = \frac{2\eta^2 - \xi^2 + 3\xi^2\eta^2}{w^6},\\
&a_5 = -\frac{u^2\eta}{\xi s^2}\, a_6 = \frac{u^2}{s^2}\, b_1 = -\frac{u^4\eta}{\xi s^4}\, b_2 = \frac{u^3\eta}{s w^4},\\
&a_7 = -\frac{\xi u\eta(3+\xi^2-2\eta^2)}{s w^6},\\
&a_8 = -\frac{u}{s}\, b_8 = p_0 = \frac{u}{s}\, p_2 = \frac{1}{sw},\\
&b_3 = \frac{\xi\eta s(3+2\xi^2-\eta^2)}{u w^6},\\
&b_7 = -\frac{2\xi^2-\eta^2-3\xi^2\eta^2}{w^6},\\
&p_1 = -\frac{\xi s^3}{u\eta}\, p_3 = -\frac{\xi s}{u^2 w^3}.
\end{aligned} \tag{B11}$$

3. *Magnetic Field Which Contributes to m*

We write down here explicitly the contributions to the magnetic field which arise from the potential Φ given by the sum of (3.6) and (3.9). From Eqs. (2.2a) and (B7) we have

$$H_\xi = \frac{(1-\eta^2)^{1/2}}{(\xi^2+\eta^2)^{1/2}}\,(f_1(\xi)\cos\varphi + f_1\perp(\xi)\sin\varphi), \tag{B12a}$$

$$H_\eta = -\frac{\eta}{(\xi^2+\eta^2)^{1/2}}\,(f_2(\xi)\cos\varphi + f_2\perp(\xi)\sin\varphi), \tag{B12b}$$

$$H_\varphi = -\frac{1}{(1+\xi^2)^{1/2}}\,(f_2(\xi)\sin\varphi - f_2\perp(\xi)\cos\varphi), \tag{B12c}$$

where the functions $f_1(\xi)$, $f_2(\xi)$ are given by

$$f_1(\xi) = H_a\xi + A_1\left(1 + \frac{1}{1+\xi^2} - \xi\arctan(1/\xi)\right), \tag{B13a}$$

$$f_{1\perp}(\xi) = A_{1\perp}\left(1 + \frac{1}{1+\xi^2} - \xi\arctan(1/\xi)\right), \tag{B13b}$$

$$f_2(\xi) = H_a(1+\xi^2)^{1/2} + A_1\left(\frac{\xi}{(1+\xi^2)^{1/2}} - (1+\xi^2)^{1/2}\arctan(1/\xi)\right), \tag{B13c}$$

$$f_{2\perp}(\xi) = A_1\perp\left(\frac{\xi}{(1+\xi^2)^{1/2}} - (1+\xi^2)^{1/2}\arctan(1/\xi)\right). \tag{B13d}$$

Terms with f_1 and f_2 represent the longitudinal part of $\mathbf{H}$ and those with $f_{1\perp}$ and $f_{2\perp}$ the transverse part.

APPENDIX C

Evaluation of $\overline{m}_2$ to $O(\varepsilon m_0)$ for a Sphere

We evaluate here the magnitude $\overline{m}_2$ for the example of an isotropic spherical superconductor with a linear $\mathbf{j}(\mathbf{v}_s)$ relation. We take the field along the z direction, since the magnetic moment m_2 is independent of this choice. As explained in the text, we must find the internal fields by solving (2.6) (which in this case reduces to the Helmholtz equation) with boundary conditions enforcing continuity of H_φ and H_θ and external fields calculated in the $\varepsilon = 0$ limit. By symmetry, $H_\varphi \equiv 0$ and we need only to impose the continuity of H_θ at the boundary, $r = a$. We obtain:

$$H_\theta \equiv -A\frac{\lambda^2}{r^3}\left(\left(1+\frac{r^2}{\lambda^2}\right)\sinh(r/\lambda) - \frac{r}{\lambda}\cosh(r/\lambda)\right)\sin\theta = \left(-H_a + \frac{m_0}{r^3}\right)\sin\theta. \tag{C1}$$

A is a constant to be determined and m_0 is given by Eq. (3.12). Since $\varepsilon = \lambda/a \ll 1$ we can approximate $\sinh(a/\lambda) \approx \frac{1}{2}e^{(a/\lambda)}$. Keeping only the leading term in the LHS of Eq. (C1) we get

$$A = 3H_a e^{-(a/\lambda)} \tag{C2}$$

and

$$H_\theta = -\frac{3}{2}H_a\frac{a}{r}e^{-(a-r)/\lambda}\sin\theta. \tag{C3}$$

We can now compute

$$\overline{\mathbf{m}}_2 = \frac{1}{8\pi}\int_\Omega d\Omega\mathbf{H}. \tag{C4}$$

Integration is performed in spherical coordinates giving

$$m_2 = \frac{1}{2}\lambda a^2 H_a = -\frac{\lambda}{a} m_0 \sim O(\varepsilon m_0). \tag{C5}$$

This result $(O(\lambda/a)m_0)$ was expected since for exponentially decaying fields, integration over the whole volume of Ω is effectively only integration over the region $\sim\lambda$ away from it surface.

ACKNOWLEDGMENTS

We thank A. Bhattacharya, A. M. Goldman, B. Bayman and B. P. Stojković for discussions concerning experimental and theoretical aspects of our work and B. F. Schaudt for help with preparing the figures. I.Ž. acknowledges support from the Stanwood Johnston Memorial Fellowship.

REFERENCES

1. L. D. Landau and E. M. Lifshitz, *Electrodynamics of Continuous Media* (Pergamon, Oxford, 1960).
2. Numerical simulations of superconductors outside of the Meissner regime are investigated in: H. G. Kaper and M. K. Wong, *J. Comput. Phys.* **119,** 120 (1995); W. D. Grapp, H. G. Kaper, G. K. Leaf, D. M. Levine, M. Palumbo and V. M. Vinokur, *J. Comput. Phys.* **123,** 254 (1996).
3. S. K. Yip and J. A. Sauls, *Phys. Rev. Lett.* **69,** 2264 (1992).
4. B. P. Stojković and O. T. Valls, *Phys. Rev. B* **51,** 6049 (1995).
5. D. Xu, S. K. Yip and J. A. Sauls, *Phys. Rev. B* **51,** 16233 (1995).
6. I. Žutić and O. T. Valls, *Phys. Rev. B* **54,** 15550 (1996).
7. N. M. Plakida, *High Temperature Superconductivity* (Springer-Verlag, Berlin, 1995).
8. J. Buan, B. P. Stojković, N. E. Israeloff, C. C. Huang, A. M. Goldman, and O. T. Valls, *Phys. Rev. Lett.* **72,** 2632 (1994).
9. F. London, *Superfluids* (Wiley, New York, 1950), Vol. 1.
10. T. P. Orlando and K. A. Delin, *Foundations of Applied Superconductivity* (Addison–Wesley, Reading, MA, 1991).
11. P. G. DeGennes, *Superconductivity of Metals and Alloys* (Addison–Wesley, Reading, MA 1989).
12. J. R. Reitz, F. J. Milfod, and R. W. Christy, *Foundations of Electromagnetic Theory* (Addison-Wesley, Reading, MA 1989).
13. J. D. Jackson, *Classical Electrodynamics* (Wiley, New York, 1975), p. 181.
14. A. Fetter and J. D. Walecka, *Theory of Many Particle Systems*, (McGraw–Hill, New York, 1971).
15. J. D. Jackson, *Classical Electrodynamics* [13] inside cover.
16. A. Bhattacharya, D. Grupp, A. M. Goldman, and U. Welp, *Appl. Phys. Lett.* **59,** 7092 (1996).
17. W. Magnus and F. Oberhettinger, *Formulas and Theorems for the Functions of Mathematical Physics* (Chelsea, New York, 1949).
18. N. N. Lebedev, *Special Functions and Their Applications* (Dover, New York, 1972).
19. W. H. Press *et al., Numerical Recipes in FORTRAN* (Cambridge Univ. Press, New York, 1992).
20. G. D. Smith, *Numerical Solution of Partial Difference Equations: Finite Difference Methods* (Oxford Univ. Press, Oxford, 1985).
21. M. K. Jain, *Numerical Solution of Differential Equations* (Wiley, New York, 1984), p. 356.
22. G. Sewell, *The Numerical Solution of Ordinary and Partial Differential Equations* (Academic Press, San Diego, 1988), p. 152.
23. Y. Saad and M. R. Schultz, *SIAM J. Sci. Stat. Comput.* **7,** 856 (1986).